ChemComm

View Online
Dynamic Article Links

Cite this: *Chem. Commun.*, 2011, **47**, 10725–10727

www.rsc.org/chemcomm

COMMUNICATION

A novel magnetic mesoporous silica packed S-shaped microfluidic reactor for online proteolysis of low-MW proteome†

Qianhao Min,[a] Xiaoxia Zhang,[a] Ren'an Wu,[b] Hanfa Zou[b] and Jun-Jie Zhu*[a]

Received 3rd July 2011, Accepted 1st August 2011
DOI: 10.1039/c1cc13969j

Magnetic mesoporous silica with a magnetic cover and mesoporous core was synthesized, filled with trypsin and located in an S-shaped microfluidic reactor. High-molecular weight (MW) proteins were split to waste by fractionation, whilst low-MW proteins were retained on the chip to be digested.

In the past decade, magnetic silica materials have triggered increasing attention in targeted drug delivery,[1] magnetic resonance imaging,[2] cell labeling,[3] and toxin separation.[4] Due to the convenience of manipulation and functionalization, magnetic silica can be considered a promising candidate for biological sample pretreatment and separation in proteome research.[5,6] Among the numerous sub-proteomes, low-MW proteome has been recently considered a rich bank for discovery of potential biomarkers and signal molecules.[7,8] In this field, mesoporous silica with magnetite core was widely applied as an absorbent for peptide enrichment with the size-exclusion mechanism to high-MW biomolecules.[9,10] However, subject to the small pore size of its perpendicular channels (2–3 nm),[9] magnetic mesoporous silica (MMS) has certain limitations as a carrier for protease in proteolysis-based proteomics. Consequently, the gap for protease reactors in low-MW proteomics was urgent to fill.

As the concept of micro total analysis systems (μTAS) spreads in analytical science,[11] microfluidic devices have emerged as a favorable tool to address biological issues in recent years. With the aim of rapid and efficient proteolysis, many endeavors have been dedicated to construct microchip reactors in proteomics.[12,13] However, apart from the single function of proteolysis, very few studies have so far been involved in the separation for specific target components of proteome/peptidome (*e.g.* low-MW proteome, phosphopeptidome and glycopeptidome), signals of which suffer the interference from other components. In our previous work,[14] size-selective proteolysis for low-MW proteome was uncovered and described by employing mesoporous silica SBA-15-SH as a tryptic reactor. Nevertheless, the digestion procedure was still performed offline in solution, suffering from the accompanied tedious sample processing.

In this work, we developed a smart S-shaped microfluidic reactor packed with MMS hybrid Fe_3O_4-SBA-15 (Scheme 1). In this tryptic microreactor, high-MW proteins could be separated to waste by automatic fractionation so that low-MW proteins were digested into peptides without the interference from the former. Other than the traditional magnetic silica with magnetic core and mesoporous silica shell, the MMS reported here is described as mesoporous silica skeleton with tiny magnetic particles coating on its external surface. In detail, Fe_3O_4 nanoparticles were synthesized by a microwave-hydrothermal technique for 30 min. As-synthesized Fe_3O_4 was given more positive charge with the aid of poly(diallyldimethylammonium chloride) (PDDA), and thus assembled to the negatively charged external surface of mesoporous silica SBA-15[15] filled with trypsin in its pore area (SBA-15-trypsin) (Fig. S1 ESI†).

As depicted in Fig. 1a and b, the Fe_3O_4 nanoparticles seem to cross the channel walls, indicating that the particles remain at the external surface instead of penetrating into the pores. In addition, as shown in its nitrogen sorption isotherm (Fig. S2a ESI†), no obvious difference was resolved in comparison with that of SBA-15 (Fig. S2b ESI†), demonstrating that the introduction of Fe_3O_4 had little effect on the pore structure. Moreover, a type-IV curve with hysteresis further verified that the pores were unblocked, and thereby could be retained for the following application. The pore size calculated from the

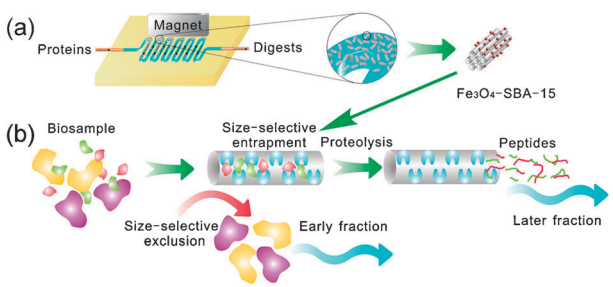

Scheme 1 (a) Schematic diagram of the MMS packed microfluidic reactor; (b) mechanism of size-selective proteolysis for protein mixture in the microfluidic reactor.

[a] *State Key Laboratory of Analytical Chemistry for Life Science, School of Chemistry and Chemical Engineering, Nanjing University, Nanjing 210093, P.R. China. E-mail: jjzhu@nju.edu.cn; Fax: (+86)-25-83597204*
[b] *CAS Key Laboratory of Separation Sciences for Analytical Chemistry, National Chromatographic R&A Center, Dalian Institute of Chemical Physics, Chinese Academy of Sciences (CAS), Dalian 116023, P. R. China*

† Electronic supplementary information (ESI) available: Experimental details, SEM, nitrogen sorption, zeta potential, MALDI-TOF MS spectra, data summary. See DOI: 10.1039/c1cc13969j

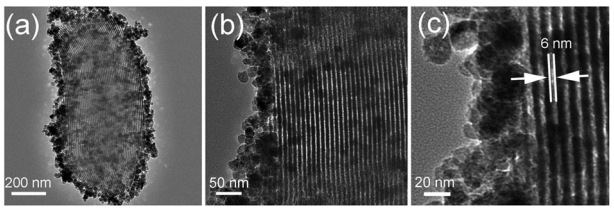

Fig. 1 TEM images of Fe_3O_4-SBA-15 hybrid.

desorption branch was 6.2 nm, comparable to the pore diameter (~6 nm) displayed in Fig. 1c. In our case, ζ potential of Fe_3O_4 was increased from 7.8 mV to 53.8 mV by addition of PDDA (Fig. S3 ESI†). Hence, the Fe_3O_4 particles were successfully attached to the negatively charged surface of SBA-15, resulting in the MMS hybrid with magnetization saturation of 28.8 emu g^{-1} (Fig. S4 ESI†), adequate for magnetic manipulation (Fig. S4, inset a ESI†). On the contrary, in the absence of PDDA, SBA-15 particles could not be isolated from the liquid phase through magnetic separation (Fig. S4, inset b ESI†), indicating failure of electrostatic assembly.

Taking advantage of the magnetism endowed by outside Fe_3O_4, we packed the magnetic beads into a glass-based microfluidic device, and then located them on the chip by an external magnet (Scheme 1a). To improve the capture efficiency of the magnetic field and prevent the leakage of stationary beads, an S-shaped channel was designed (S5 ESI†). In the normal linear channel, vertical to the magnetic force direction, fluid force on the beads has to be balanced by the static friction from the channel wall, which depends on magnetic force and static friction coefficient (μ, in most case, $\mu < 1$) (Scheme S1a ESI†). Instead, S-shaped channel could directly counterbalance fluid force by magnetic force because they parallel each other (Scheme S1b ESI†). As a result, the hybrid was readily immobilized in the bent channels as well as straight channels with a flow direction opposite to the magnetic field (S5 a and b ESI †). In our case, the first two bends of an S-shaped channel were packed with MMS beads, and the downstream bends reserved to hold the beads which leaked from upstream. This multiple capture mode enhanced the efficiency of bead immobilization, and minimised the chance of clogging downstream in the microcolumn. In the case of the linear chip, some brown packed beads were washed out at a flow rate of only 2 μL min^{-1}, while the S-shaped channel could sustain a flow rate up to 10 μL min^{-1}. Ultimately, two capillary tubes were equipped at both sides of the chip for compatibility with subsequent applications for online LC-MS.

Size-selective proteolysis was proposed in our previous study as preferential digestion for low-MW proteins owing to the size-exclusion effect of the trypsin reactor. In this study, we utilized trypsin-encapsulated MMS as the stationary phase for size-exclusion separation as well as size-selective proteolysis, with high-MW proteins excluded for isolation in the early fraction and low-MW proteins digested into peptides in the later fraction (Scheme 1b). A protein mixture of Cytochrome *c* (Cyt *c*, MW = 12384 Da, 2.6 × 3.2 × 3.3 nm^3) and bovine serum albumin (BSA, MW = 66400 Da, 5.0 × 7.0 × 7.0 nm^3)[16] at the same concentration of 5 pmol μL^{-1} was employed as substrate for the tryptic microreactor. A flow rate of 1 μL min^{-1} was adopted for the injection of 20 μL protein sample, and the eluent was collected at the outlet of microchip as an early fraction. Afterwards, 20 μL of 10 mM NH_4HCO_3 (pH = 8.0) buffer solution followed at flow rate of 2 μL min^{-1}, with eluent named as a later fraction. Both early and later fractions driven out from capillary tube were collected for MALDI-TOF MS analysis. For comparison, in-solution digestion was also performed for the mixture. As shown in Fig. 2a, conventional digestion led to an overwhelming 29 peptides derived from BSA and only 2 peptides from Cyt *c* (Table S1 ESI†, peptide data summary was attached in the ESI†). After using the microfluidic reactor, 5 peaks at a fairly low signal-to-noise ratio (S/N) were resolved in the early fraction (Fig. 2b). But for the later fraction, abundant peptide information and improved peak S/N could be obtained (Fig. 2c). Only 3 peptides were assigned to BSA, while the peptides of Cyt *c* were enhanced from 2 to 13 in comparison to in-solution strategy. This discrimination of proteolysis in the microreactor elucidated that low-MW protein Cyt *c* was digested first rather

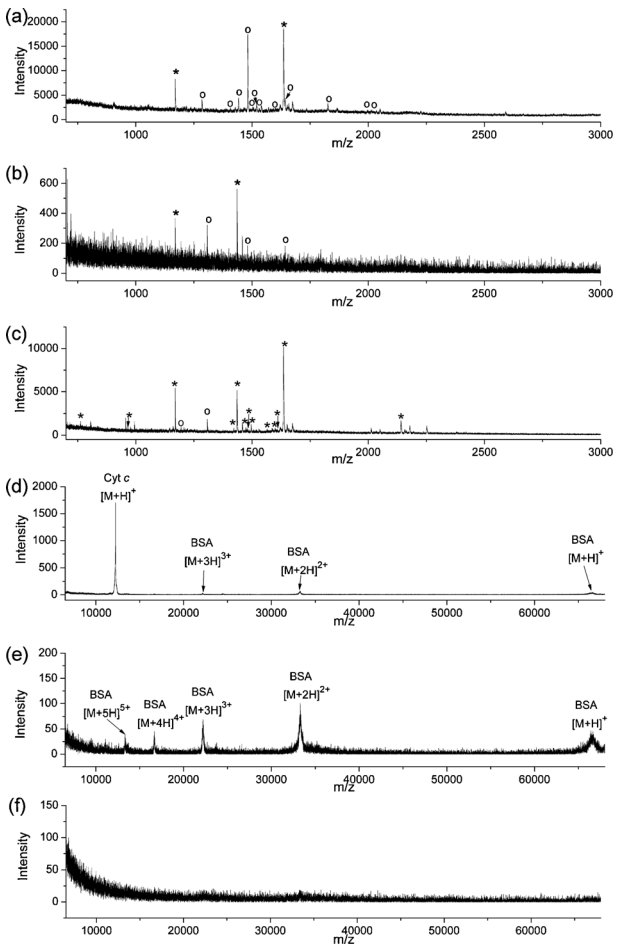

Fig. 2 MALDI-TOF spectra of peptides from mixture of Cyt *c* and BSA by (a) in-solution digestion and (b,c) on-chip digestion ((b) for the early fraction; (c) for the later fraction). MALDI-TOF spectra of proteins from mixture of Cyt *c* and BSA (d) before and (e,f) after on-chip digestion ((e) for the early fraction; (f) for the later fraction). Peptide peaks at relatively high S/N are labeled with an asterisk and circle. An asterisk is assigned to peptides from the digest of Cyt *c*; a circle is assigned to peptides derived from BSA.

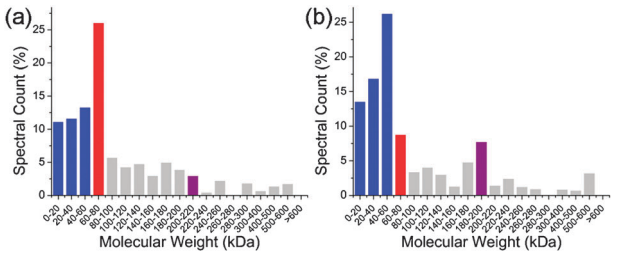

Fig. 3 Spectral count percentage distributions *versus* the MW of proteins identified in human serum by (a) in-solution digestion and (b) on-chip digestion.

than high-MW protein BSA, resulting from the size-selective effect of the packed beads Fe_3O_4-SBA-15 in the microchip. Meanwhile, in the high m/z section, several multiple-charged ions of intact BSA were detected in the early fraction (Fig. 2e), while the peak of Cyt *c* was removed compared to the spectrum of the initial protein mixture (Fig. 2d). This demonstrated that low-MW protein Cyt *c* was entrapped in the packed bed, whereas high-MW protein BSA was washed out of the reactor along with the fluid. Ascribed to the retention of Cyt *c* in the reactor bed, the digestion process was delayed in comparison with the early fraction. As a result, its peptides were released into the later fraction rather than the early one, generating the difference of peptide information between them as mentioned above (Fig. 2b and c). In addition, as BSA flowed out with early fraction in advance, the intact protein background was eliminated in the spectrum of the later fraction (Fig. 2f). Replacing Cyt *c* by other model proteins (lysozyme, MW = 14 388 Da, 1.9 × 2.5 × 4.3 nm^3 or myoglobin, MW = 17 000 Da, 2.1 × 3.5 × 4.4 nm^3), similar results were achieved for both fractions (Fig. S6 and S7 ESI†). By this procedure, high-MW intact proteins could be directly separated from the peptides of low-MW proteins through fractionation in the microreactor.

Another attractive merit of the microreactor is rapid and automatic analysis for biological samples. To demonstrate this advantage, the microfluidic device was integrated into the LC-MS system for online proteolysis of a real sample human serum (Scheme S2 ESI†). Following database searching, a spectra counting method[17] was used to semi-quantify the proteins identified. As shown in Fig. 3a, by conventional digestion, proteins ranging from 60–80 kDa dominate the spectral count distribution. However, by using the microreactor, proteins in this range were declined by a significant margin, along with the enhancement of proteins with a MW less than 60 kDa (Fig. 3b). In particular, the spectral count of human serum albumin (HSA), the highest protein content in human serum,[7] dropped dramatically from 1034 to 48 (Table S4 ESI†, see data summary in ESI†). Note that the enhancement at 180–200 kDa by on-chip digestion, which goes against the size-selective effect, was attributed to the peptides of Complement C3 generated by endogenous protease in the crude biosample.[18] In this strategy, low-MW proteins in human serum could be more confidently identified, suggesting the great potential of the MMS packed microfluidic reactor for online analysis of low-MW biomolecules in complex samples. More significantly, in this integrated microdevice for programmed sample loading, digestion, fractionation and LC-MS analysis time consumption could be reduced to only 2.5 h, compared to 18 h by our previous offline protocol,[16] including digestion, desalting, lyophilization and LC-MS analysis.

In summary, a magnetic mesoporous silica hybrid was synthesized by electrostatically assembling Fe_3O_4 nanoparticles onto the negatively charged substrate SBA-15 with the aid of PDDA, and packed into an S-shaped glass microchip reactor as the host of protease. Owing to the S-shaped design, capture performance of the magnetic beads was remarkably enhanced. Given the size-exclusion effect from the component of SBA-15, the microfluidic reactor could be applied in proteolysis of low-MW proteins as well as separation of high-MW proteins. Moreover, due to its rigid base and robust interface, the microdevice could be directly connected into LC-MS for protein fractionation, synchronous digestion, gradient elution and MS detection, offering great promise for realizing online analysis and automatic operation in proteome research.

The work was supported by National Natural Science Foundation of China (No. 21020102038, 20821063, 20875089) and 973 Program (No. 2011CB933502).

Notes and references

1 F. H. Chen, L. M. Zhang, Q. T. Chen, Y. Zhang and Z. J. Zhang, *Chem. Commun.*, 2010, **46**, 8633–8635.
2 J. E. Lee, N. Lee, H. Kim, J. Kim, S. H. Choi, J. H. Kim, T. Kim, I. C. Song, S. P. Park, W. K. Moon and T. Hyeon, *J. Am. Chem. Soc.*, 2010, **132**, 552–557.
3 C. W. Lu, Y. Hung, J. K. Hsiao, M. Yao, T. H. Chung, Y. S. Lin, S. H. Wu, S. C. Hsu, H. M. Liu, C. Y. Mou, C. S. Yang, D. M. Huang and Y. C. Chen, *Nano Lett.*, 2007, **7**, 149–154.
4 H. Y. Lee, D. R. Bae, J. C. Park, H. Song, W. S. Han and J. H. Jung, *Angew. Chem., Int. Ed.*, 2009, **48**, 1239–1243.
5 S. Lin, G. P. Yao, D. W. Qi, Y. Li, C. H. Deng, P. Y. Yang and X. M. Zhang, *Anal. Chem.*, 2008, **80**, 3655–3665.
6 Z. Zou, M. Ibisate, Y. Zhou, R. Aebersold, Y. Xia and H. Zhang, *Anal. Chem.*, 2008, **80**, 1228–1234.
7 N. L. Anderson and N. G. Anderson, *Mol. Cell. Proteomics*, 2002, **1**, 845–867.
8 R. S. Tirumalai, K. C. Chan, D. A. Prieto, H. J. Issaq, T. P. Conrads and T. D. Veenstra, *Mol. Cell. Proteomics*, 2003, **2**, 1096–1103.
9 S. S. Liu, H. M. Chen, X. H. Lu, C. H. Deng, X. M. Zhang and P. Y. Yang, *Angew. Chem., Int. Ed.*, 2010, **49**, 7557–7561.
10 J. H. Wu, X. S. Li, Y. Zhao, Q. A. Gao, L. Guo and Y. Q. Feng, *Chem. Commun.*, 2010, **46**, 9031–9033.
11 A. Manz, N. Graber and H. M. Widmer, *Sens. Actuators, B*, 1990, **1**, 244–248.
12 Y. Liu, H. X. Wang, Q. P. Liu, H. Y. Qu, B. H. Liu and P. Y. Yang, *Lab Chip*, 2010, **10**, 2887–2893.
13 A. G. Pereira-Medrano, S. Forster, G. J. S. Fowler, S. L. McArthur and P. C. Wright, *Lab Chip*, 2010, **10**, 3397–3406.
14 Q. H. Min, R. A. Wu, L. A. Zhao, H. Q. Qin, M. L. Ye, J. J. Zhu and H. F. Zou, *Chem. Commun.*, 2010, **46**, 6144–6146.
15 D. Y. Zhao, J. L. Feng, Q. S. Huo, N. Melosh, G. H. Fredrickson, B. F. Chmelka and G. D. Stucky, *Science*, 1998, **279**, 548–552.
16 M. Hartmann, *Chem. Mater.*, 2005, **17**, 4577–4593.
17 J. Gao, G. J. Opiteck, M. S. Friedrichs, A. R. Dongre and S. A. Hefta, *J. Proteome Res.*, 2003, **2**, 643–649.
18 X. Y. Zheng, H. Baker and W. S. Hancock, *J. Chromatogr., A*, 2006, **1120**, 173–184.